Strength Assessment of Stiffened-Panel Structures against Buckling Loads: FE Benchmarking and Analysis

M. Sholikhah [1], R. Ridwan [2*], A. R. Prabowo [1*], T. Ghanbari-Ghazijahani [3],
I. Yaningsih [1], N. Muhayat [1], D. D. D. P. Tjahjana [1], R. Adiputra [4], J. M. Sohn [5]

[1] Department of Mechanical Engineering, Universitas Sebelas Maret, Surakarta, Indonesia.

[2] Department of Mechanical Engineering, Universitas Merdeka Madiun, Madiun, Indonesia.

[3] Faculty of Science and Engineering, School of Engineering, Macquarie University, New South Wales, Australia.

[4] Research Center for Hydrodynamics Technology, National Research and Innovation Agency (BRIN), Surabaya, Indonesia.

[5] Department of Naval Architecture and Marine Systems Engineering, Pukyong National University, Busan, South Korea.

Abstract

This research endeavors to examine the effect of stiffener shapes on the structural capacity of stiffened-plate structures, specifically focusing on Tee (T), Angle (L), and Flat (I) stiffened plates. The primary objectives are threefold: firstly, to quantify the critical load values during the buckling phenomenon for T, L, and I stiffened plates; secondly, to assess model deformation upon failure; and thirdly, to investigate whether the buckling behavior of T, L, and I stiffened plates correlates with distinct failure patterns. Employing numerical simulation through the finite element method, this study sheds light on previously unexplored aspects of structural behavior. The findings indicate that angle stiffeners exhibit superior load-bearing performance compared to flat bars. Notably, the research reveals a substantial increase in maximum compressive load by at least 15.90% with Tee bar and 8.25% with angle bar stiffeners when the stiffened panels undergo a 5 mm displacement, presenting a potential avenue for structural enhancement. Additionally, the study demonstrates that T bars outperform in terms of resisting buckling. Noteworthy is the novel approach of examining the combined effect of transverse frame, longitudinal frame, and hull girder under buckling scenarios, a facet not explored in previous research. Furthermore, the utilization of steel S355JR-EN10210 as a material introduces a unique dimension not previously considered in these scenarios.

Keywords: Ultimate Strength; Stiffened Panel; Buckling Load; Ship Structure; Nonlinear Finite Element Method (NLFEM).

1. Introduction

Ships play a crucial role on a global scale and are an essential element of international commerce. By 2020, nearly 10.7 billion tons of international maritime trade were carried out. Nevertheless, this figure is marginally reduced compared to 2019 as a result of the sequential disruptions caused by the COVID-19 pandemic in supply chains, demand, and logistics. The COVID-19 pandemic has proven to be disrupting maritime transport, although the results are less damaging than previously feared. In the year 2019, the global maritime trade amounted to 11.2 billion tons. Contrary to predictions, the decline in volume during 2020 was less severe than anticipated. By year-end, there was a recovery, setting the stage for a significant shift in worldwide supply chains and the emergence of novel patterns in maritime trade.

The disruptions in the initial half of 2020 led to a contraction of 3.8 percent in maritime trade for the year [1]. Not only that, safety and shipping studies show that there will be 49 missing ships by the end of 2020 worldwide. All in all, in 2019, it was reported that there were 48 missing ships that occurred worldwide [2]. Various factors contribute to this catastrophe, including but not limited to fire or explosion, collisions, grounding, hull impairment, and engine malfunction or failure.

Numerous authors have delved into the investigation of buckling and post-buckling phenomena in thin-walled structures exposed to buckling loads. Among them, Paik & Seo [3] and Omidali & Khedmati [4] focused their research on the thin-walled structures' stability. Paik & Seo [3] contributed valuable insights by applying nonlinear finite element methods (NLFEM) to assess the Ultimate Limit State (ULS) of steel stiffened-plate structures. Their exploration involved utilizing lateral pressure actions and biaxial compression to evaluate the ultimate strength of the panels. Doan et al. [5] conducted a strength assessment of panels made of stiffened aluminium and steel, featuring openings on longitudinal girders under compressive loads. Employing finite element analyses, they provided a detailed description of the models' deformation. Pedram & Khedmati [6] utilized finite element analyses to investigate how welding affects the strength of aluminium-stiffened plates under the influence of both uniaxial compression and lateral pressure. The study incorporated common marine aluminium alloys with mechanical and geometrical imperfections in the stiffened panel. In a case study without finite element analyses, Guedes Soares and Gordo [7] introduced approaches for designing stiffened plates subjected primarily to uniaxial compression. Their approach utilized the method outlined by the American Bureau of Shipping (ABS) to determine buckling strength.

In recent years, researchers have shown a keen interest in the subject of dynamic buckling. An illustrative example is the study conducted by Feng et al. [8]. The study concentrated on conducting a compression test on hull plates to evaluate the influence of interconnected damage on their ultimate strength. Using AH36 steel material, the research investigated the ultimate strength of hull plates affected by both pitting corrosion and cracks simultaneously. Cui & Wang [9] undertook both numerical and experimental examinations of the capacity of corrugated and plane bulkheads subjected to lateral pressure. Their study, employing corrugated stiffener types, revealed that when a corrugated bulkhead deforms under lateral pressure, the flange on the bulge side primarily experiences tensile stress, while the flange on the opposite side bears compressive stress. Lee & Kang [10] explored the elastic local buckling factors of I-shaped beams with a focus on flange-web interaction. Their study aimed to comprehend the local buckling characteristics and strength of I-shaped structural sections using three-dimensional finite element analysis, with a specific emphasis on the interactions between flanges and webs. Another study conducted by Boissonnade et al. [11] employed both experimental and numerical approaches to investigate buckling, utilizing cellular steel beams as structures. Moreover, Ghadami et al. [12] investigated the buckling and post-buckling characteristics of I-beams with coped top flanges and slender web panels. Their study investigated the influence of plate slenderness, cope specifications (depth, length), and initial geometric imperfections on the elastic, inelastic, and post-buckling responses of such beams. Stiffened panel structures featuring flat, angle, and Tee bar stiffeners play a pivotal role in marine engineering, thin-walled structures, particularly within the domain of ship construction. These distinct stiffener types are strategically employed to enhance the structural integrity and strength of ship components, ensuring optimal performance under varying maritime conditions. Observing that the majority of investigations into the buckling phenomenon concentrate primarily on the hull plate structure, it is evident that these studies overlook the interactions among the plate, various stiffener types (L, T, I), transverse frame, longitudinal girder, and the specific marine steel grade material used.

The major aim of this investigation was to look into the behavior of stiffened plates subjected to buckling loads, with a comprehensive consideration of various stiffener types, namely angle, flat, and Tee bar, in conjunction with the influential factors of transverse frames and longitudinal girders. Notably, the study employed S355JR-EN10210 steel as the material of choice, introducing a critical element to the analysis that had not been previously explored in this context. Additionally, a numerical modeling approach employing the FE method was implemented. The reliability and precision of this numerical model were established through a benchmarking study, aligning the simulated outcomes with experimental results. Moreover, this study placed an emphasis on scrutinizing the failure mechanisms inherent in stiffened plates under the influence of buckling loads, as simulated through the finite element method.

2. Research Methodology

2.1. Benchmarking

The inclusion of a benchmarking study in the research methodology serves as a critical measure to guarantee the reliability and robustness of the obtained results by validating the numerical simulations against established reference values or experimental data. Tests of stiffened panels that have been performed by Quinn et al. [13] will become benchmarking studies in this study. Figure 1a shows the specimen geometry and the dimensions of the stiffened panel. The specimen has an arrangement with twelve sub-stiffeners and three stringers, each 590 mm long. The stringers possess a height and thickness of 28 mm and 2.8 mm, respectively, parallel at 167 mm apart.
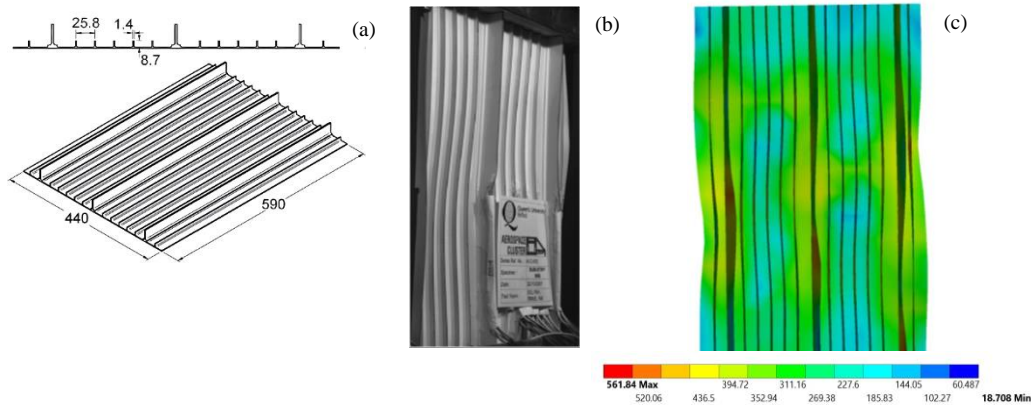
Figure 1. (a) The dimension of the stiffened plate [13]; (b) deformation mode in the experiment [8]; and (c) deformation mode in the numerical finite element.

The sub-stiffeners, measuring 8.7 mm in height and 1.4 mm in thickness, are positioned between the longitudinal stringers. The plating exhibits a thickness of 2.2 mm. Utilizing Aluminium Alloy 2024-T351, specimens were fabricated for experimental testing. A hydraulic testing machine with a 500 kN capacity conducted the tests.

In this study, the material properties of aluminium alloy (2024-T3) were assumed and used since the ones of 2024-T351 were not mentioned in the study conducted by Quinn et al. [13]. The 2024-T3 has materials features as follows: density ρ of 2780 kg/m^3, Young's modulus E of 73.4 GPa, Poisson's ratio v of 0.33, Yield stress σ_y of 315 MPa, Tensile strength σ_u of 550 MPa, and failure strain ε_f 0.18 [14, 15]. The ones for 2024-T3 are presented in Table 1. A comparison of the total mass stiffened panel to the original (as calculated by Quinn et al. [13]) and the proposed stiffened panel is presented in Table 2. It is observed that they correlated well and had no significant deference compared to the experimental data. The current stiffened panel has a total mass of 1.993 kg in comparison to the test data of 1.968 kg. Hence, the mass percentage difference is lower than 1.27% if compared to the tests.

Table 1. Material features of 2024-T3

Property	Symbol	Value
Density	ρ	2780 kg/m^3
Yield stress	σ_y	315 MPa
Young's modulus	E	73.4 GPa
Tensile strength	σ_u	550 MPa
Poisson's ratio	v	0.33
Exponent	n	0.406
Failure strain	ε_f	0.18

Table 2. Mass comparative study of the stiffened plate

Data Source	Mass	Mass Difference	Mass Difference (%)
Quinn et al. [13]	1.968 kg	-	-
Current study	1.993 kg	+0.025 kg	+1.27 %

The calculations are executed utilizing the ANSYS commercial software for finite element analysis [16]. The deformation mode obtained from the numerical finite element seems in accordance with the experimental data in Figures 1b and 1c. The load versus displacement is shown in Figure 2. The examination of mesh convergence has been carried out on stiffened panels of varying dimensions, ranging from 40 to 60 mm in the finite element analysis. As shown in Figure 2, the load versus displacement curves for all element sizes are extremely similar to experimental results. Quinn et al. [13] found that the capacity of the experimental buckling of the stiffened panel showed at 255 kN. Here, the 40, 45, 50, 55, and 60 mm of element sizes produce the ultimate strength of 258.43, 250.74, 253.86, 252.18, and 238.81 kN, respectively. It is observed that the error produced by these element sizes does not exceed 6.6%. The choice of a 60-mm mesh size is based on a careful consideration of both computational time and accuracy, as illustrated in Figure 2. This mesh size is sufficiently small to accurately capture the deformation of the model.
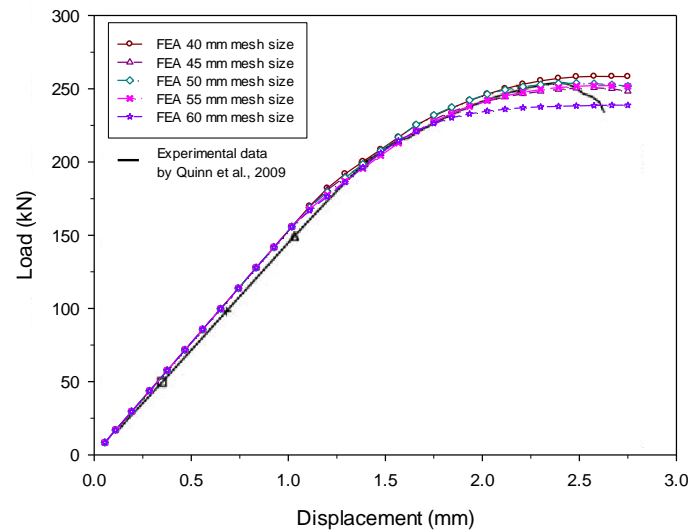
Figure 2. Mesh sensitivity study of the stiffened plate obtained through finite element analysis

2.2. Model and Boundary Conditions

An ANSYS software is utilized to construct a finite element model with non-linear characteristics [16] for simulating the buckling scenarios of stiffened panels. A 4200 × 24000 mm stiffened panel similar to the one used in the work of Doan et al. [5] is used for the buckling scenario. Figure 3 presents the details of the dimension. The stiffened panel consists of the plate, stiffener, transverse frame and longitudinal girder. Dimension of the plate is observed at width and length of 2400 mm and 4200 mm, respectively. The longitudinal girder is made with the Tee bar type with a stiffener size in height $h_w = 150$ mm, web thickness of stiffener $t_w = 8$ mm, flange breadth of stiffener $b_f = 100$ mm, and flange thickness of stiffener $t_f = 10$ mm. Twelve stiffeners attached to the plate have the dimensions of $h_w = 60$ mm and thickness $t_w = 6$ mm. In this study, the transverse frame is modelled with different stiffeners i.e., angle, flat, and Tee bar and the resulting stiffened panel strength will be assessed for the three types of stiffeners. Typical three types of stiffeners that are commonly used in marine structures are shown in Figure 4.
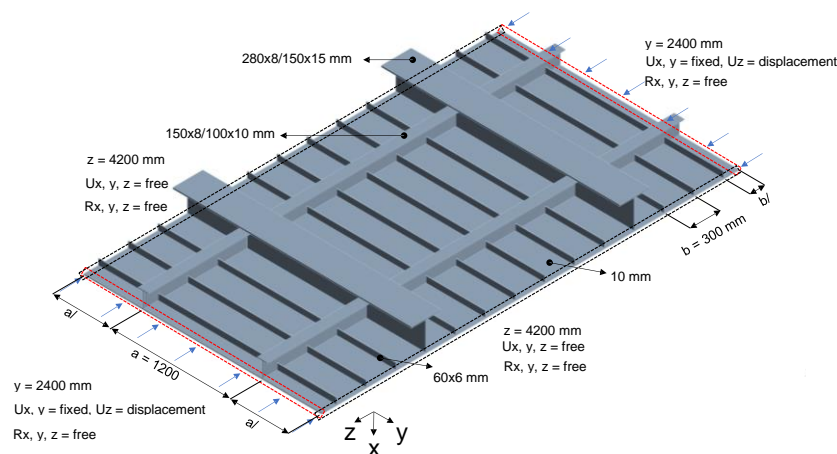

Figure 3. The dimension of a stiffened-plate structure [5]
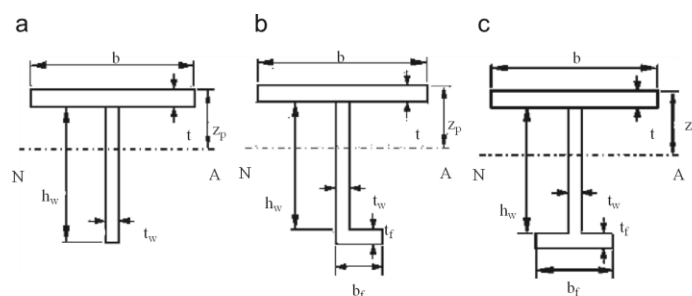

**Figure 4. (a) Flat; (b) angle; and (c) Tee bar stiffeners [3]**

Table 3 summarizes the geometrical properties of the stiffened panels. For both plating, longitudinal girder, and stiffeners, the S355JR-EN10210 steel becomes the manufacture-grade material. S355JR-EN10210 steel has Young's modulus $E = 210$ GPa, the density $\rho = 7800$ kg/m^3, Poisson's ratio $v = 0.3$, and failure strain $\varepsilon_f = 0.28$. The yield stress σ_y and ultimate stress σ_u are 390 MPa and 495 MPa, respectively. The strain hardening exponent (n) and strength coefficient (K) are 0.18 and 830 MPa, respectively. Common steel materials including the mechanical properties used in the finite element analysis can be found in the study conducted by Ridwan et al. [17].

Table 3. Stiffened panels and their geometric dimensions

Panel	a (mm)	y (mm)	z (mm)	b (mm)	t (mm)	h_w (mm)	t_w (mm)	b_f (mm)	t_f (mm)
Flat bar	1200	2400	4200	300	10	150	8	-	-
Angle bar	1200	2400	4200	300	10	150	8	50	10
Tee bar	1200	2400	4200	300	10	150	8	100	10

The boundary condition is an essential part of finite element analysis [18, 19]. Therefore, in this study, applied boundary conditions to the stiffened panel are such as translation constraint, displacement, and rotation constraint. The translation constraints are set at Ux, and Uy at each end of the specimen at coordinates $z = 0$ mm and $z = 4200$ mm. Displacement in the Uz direction is made free at both ends of the specimen to apply the buckling phenomenon. On both sides of the stiffened panel, the translation and rotation constraint are made in Ux, Uy, Uz = free and Rx, Ry, Rz = free. The simulation time is performed at 1 s. The boundary condition applied on buckling of the stiffened panel is shown in Figure 3. The three different types of stiffener models applied to the transverse frame are assessed in this study to measure their effect on buckling on stiffened panels. The stiffeners are modelled with the flat, angle, and Tee bar, Figure 4. For flat bar, the thickness t_w is set to be 8 mm in height h_w 150 mm. As for the angle and Tee bars, the size is stiffener flange breadth $b_f = 50$ mm and 100 mm dan and stiffener flange thickness t_f made in 10 mm, respectively. The geometric characteristics of the reinforced panels examined in the current investigation are summarized in Table 3.

The buckling scenario was simulated through the utilization of the nonlinear finite element method (NLFEM) in this analysis. The first step of the research is to create the specimen in ANSYS Workbench, which allows the geometric representation and the structural components to be defined in the software. Next, the material properties are assigned, using S355JR-EN10210 steel as the material model for the specimen. Then, the mesh size is carefully determined, which is essential for obtaining accurate and reliable numerical simulations. After that, the boundary conditions are specified, including the constraints and loading conditions that simulate the buckling load. The fifth step is to define the solution parameters, which include the analysis of stress, strain, and deformation patterns in the specimen. This stage enables a comprehensive understanding of the structural response under different conditions. This sequential approach ensures a systematic and methodical execution of the research, which helps to study the behaviour of stiffened plates under buckling loads. Figure 5 shows the flowchart in this research.
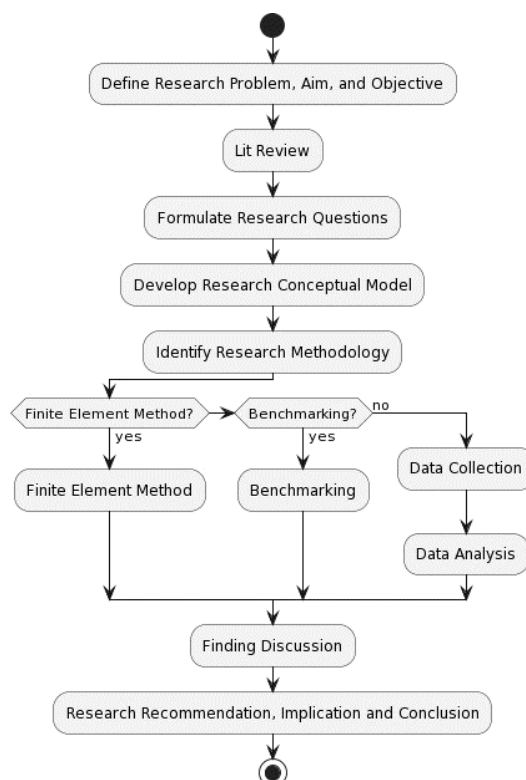
Figure 5. Flowchart presenting the research steps

3. Results and Discussion

3.1. The Stiffeners and Their Effects

Figure 6 shows the comparison of the ultimate compressive strength of stiffened panels subjected to 5 mm displacement with flat, angle, and Tee bar. As shown in Figure 6, the stiffener with the Tee bar type appears to have a maximum load that is greater than the angle and Flat bar. However, at 0 to 1.8 mm displacement seems to have a fairly equal load that can be endured for all three types of stiffener. Upon surpassing a displacement threshold of 1.8 mm, a discernible contrast in load resistance becomes apparent, wherein flat bars exhibit the least capacity when juxtaposed with Tee bars and Angle bars. The maximal compressive strength generated by these three stiffeners manifests as 6191.3 kN for flat bars, 6702.2 kN for angle bars, and 7176 kN for Tee bars, underscoring the substantial disparities in their load-bearing capabilities beyond the specified displacement threshold.
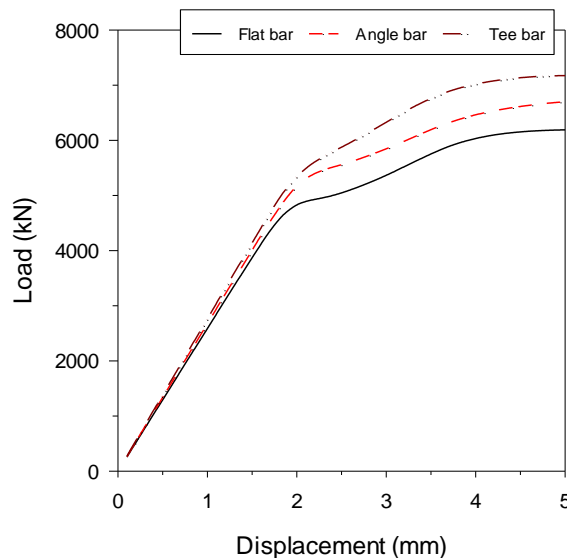

Figure 6. Capacity of stiffened panels with 5 mm displacement.

As it is observed, the maximum compressive strength increases by 15.90 % and 8.25 % for the Tee and angle bar type compared to the flat bar, respectively. The ultimate strength of stiffened panels with 10 mm displacement is presented in Figure 7. It seems that the load versus displacement obtained from 10 mm of displacement is not quite different from the 5 mm of displacement. There are some increases in terms of maximum compressive strength obtained from flat, angle, and Tee bars. Upon observation, it is noted that the maximum compressive strength generated on the ribs of this stiffener manifests as 6297.5 kN, 6832.8 kN, and 7292 N, respectively. Significantly, a discernible enhancement is evident, with the maximum compressive strength increasing by 8.50% and 15.79% for the Tee bar and angle bar types in comparison to the flat bar, respectively. It is noteworthy that this percentage increase remains consistent when subjected to a 5 mm displacement, indicating a sustained and consistent improvement in compressive strength across the different stiffener types, thereby emphasizing the stability and reliability of the observed trends.
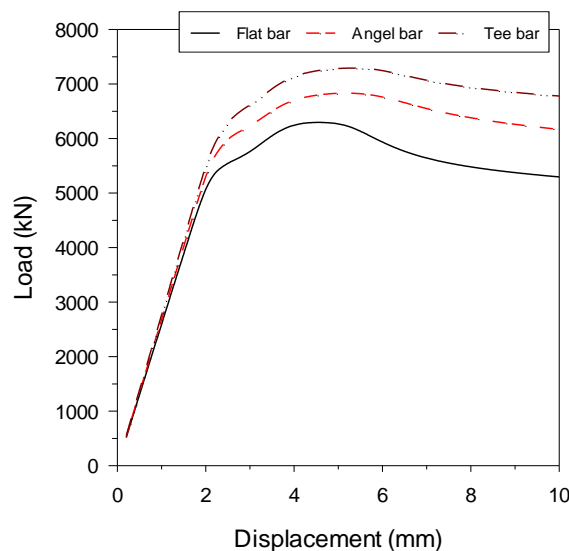

Figure 7. Ultimate strength of stiffened panels subjected to 10 mm displacement

Different things happened to the average stress generated from the three different stiffeners (Figures 8 and 9). Deformation shapes and von-Mises stress of panels subjected to 5 mm and 10 mm of displacement are presented in Figures 10 and 11, respectively. At 5mm displacement, the average stress produces a fairly similar stress result for the three stiffeners. The resulting values are 250.81 MPa, 254.08 MPa, and 249.8 MPa produced from stiffener-type flat, angle, and Tee bar, respectively. This shows that no more than a 1.30 % difference occurs. Significant variations become apparent when a 10mm displacement is applied, as depicted in Figure 9. These disparities manifest when the displacement exceeds 5mm. Among the stiffeners examined, the Tee bar exhibited the highest maximum average stress, measuring approximately 255.94 MPa, followed closely by the angle bar at 249.71 MPa and the flat bar at 240.66 MPa. This translates to percentage increments of about 3.76% and 6.35% for the angle and Tee bars in comparison to the flat type. Moreover, as depicted in Figure 12, the visual representation showcases the equivalent strain distribution within a stiffened panel upon the culmination of the simulation, taking into account both 5 mm and 10mm displacements. Notably, the discernible observation emerges that irrespective of the stiffener type—be it the flat bar, angle bar, or Tee bar—the obtained results exhibit a striking uniformity in terms of maximum strain. This uniformity is distinctly evident, with the maximum strain values converging within the narrow range of 0.0028 to 0.003 for the 5 mm displacement scenario and 0.0034 to 0.0037 for the 10 mm displacement scenario.
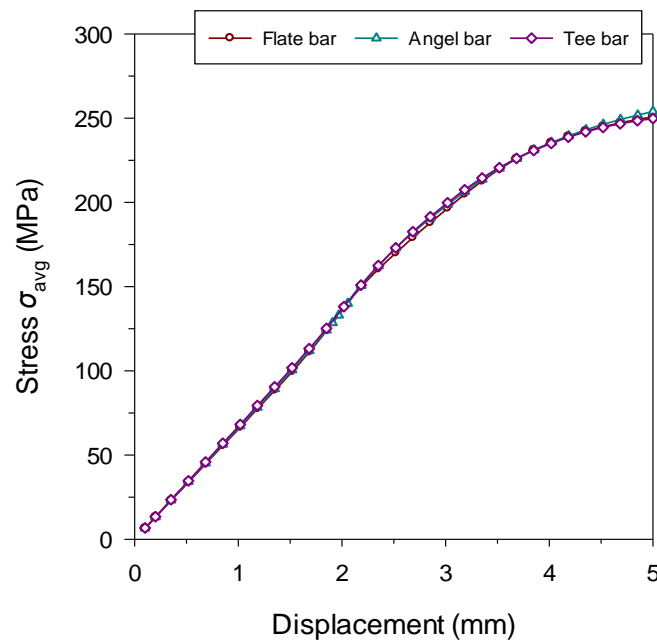

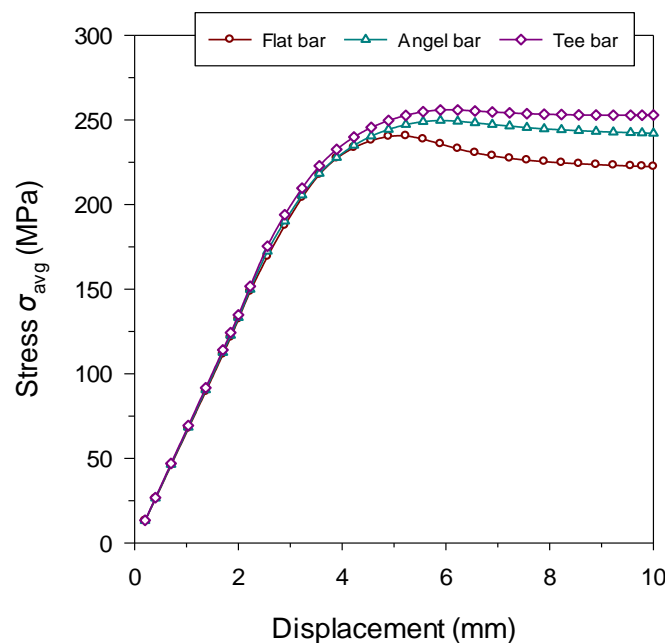**Figure 8. Stress average of stiffened panels subjected to 5 mm displacement**

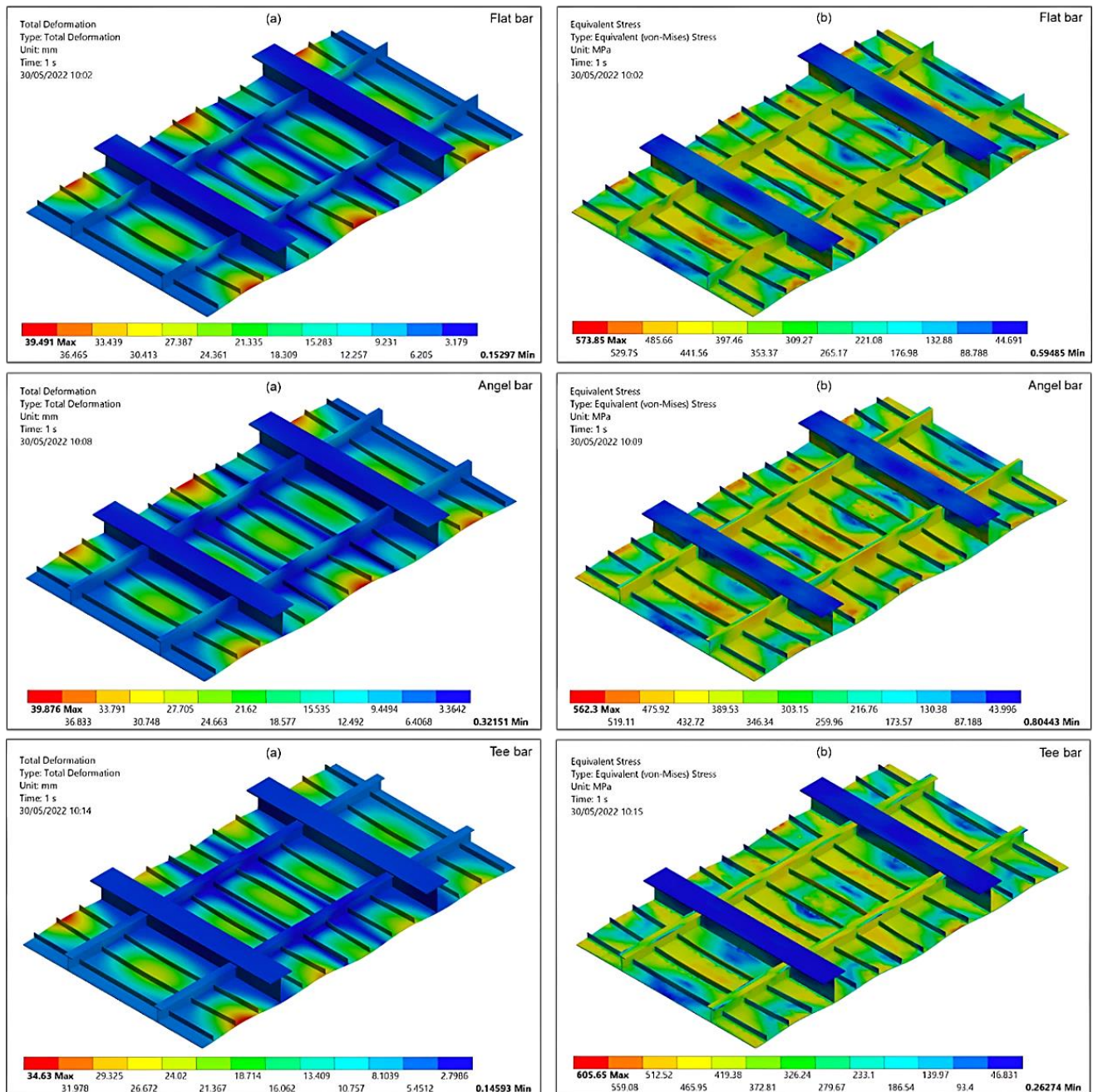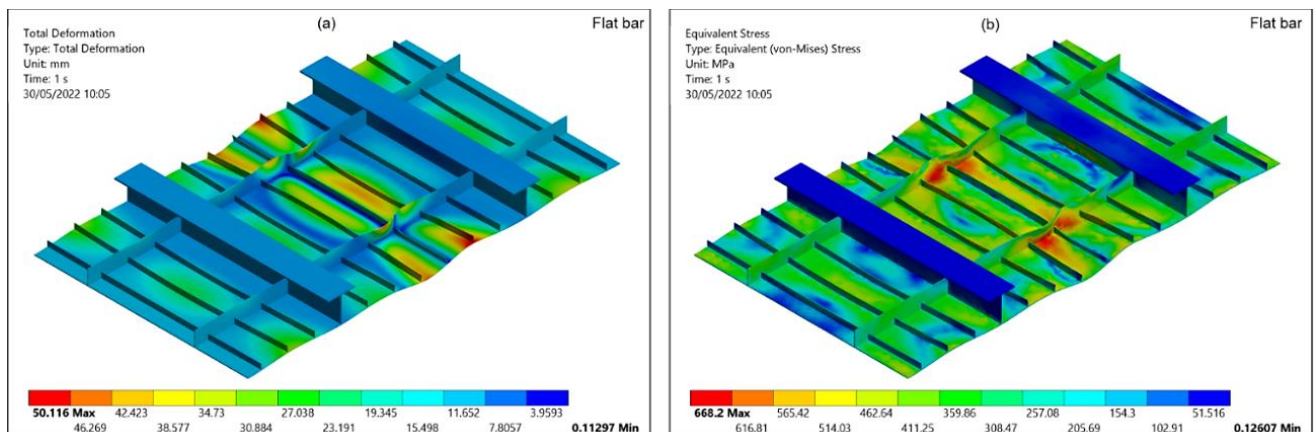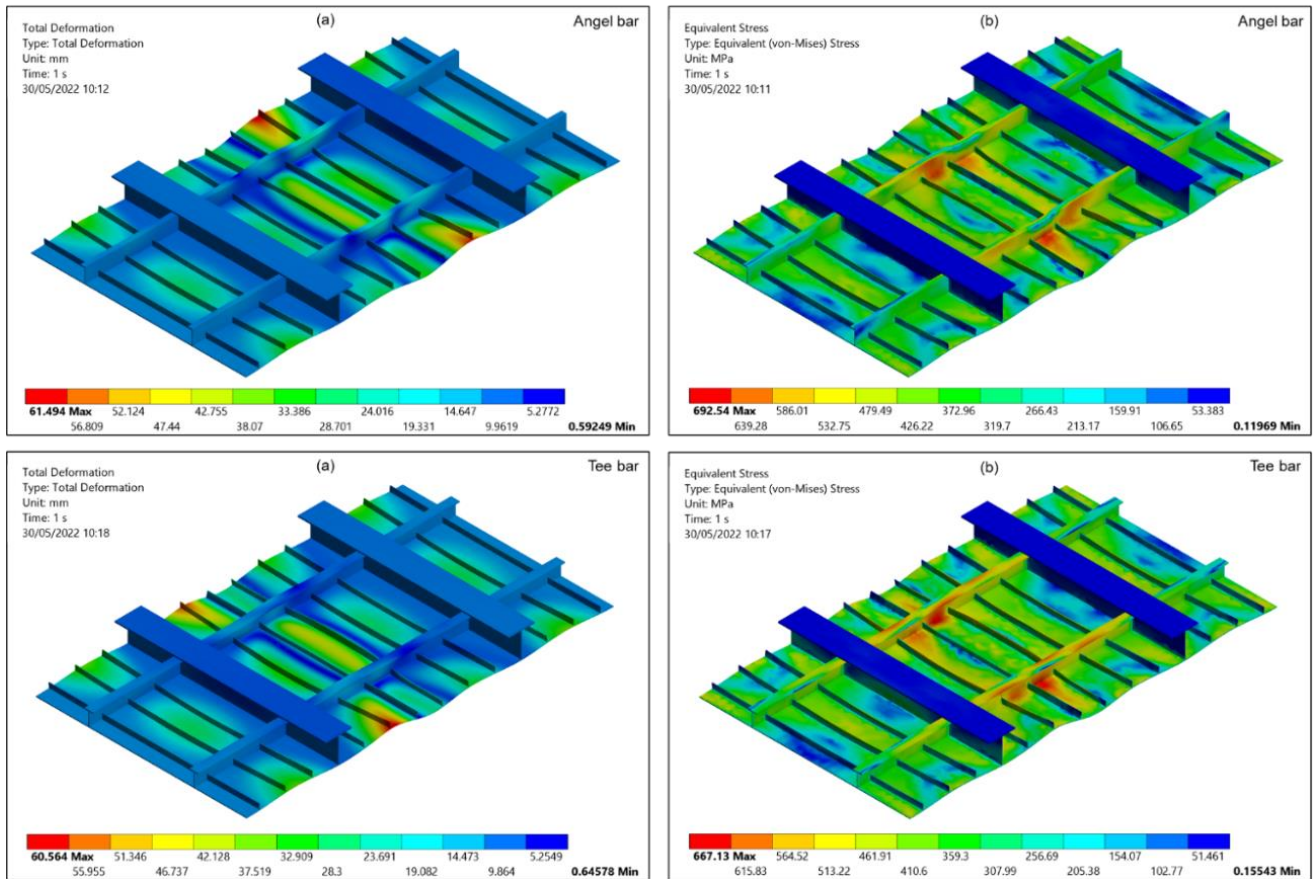**Figure 9. Stress average of stiffened panels subjected to 10 mm displacement**

Figure 10. Deformation shapes and von-Mises stress distributions of stiffened panel subjected to 5 mm displacement: (a) Total deformation; and (b) Von-Mises stress contour
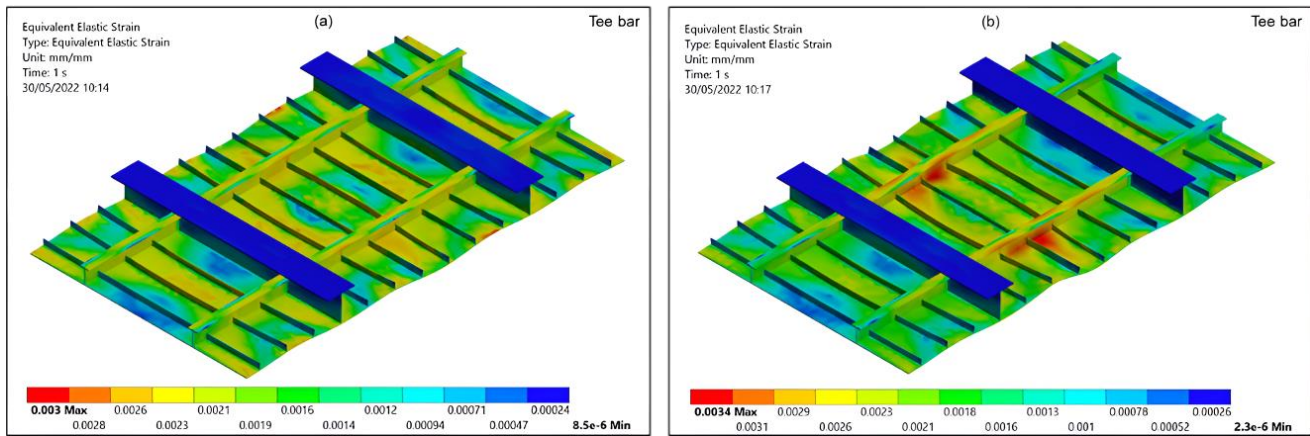
Figure 11. Deformation and stress (von-Mises) of panel subjected to 10 mm displacement: (a) Total deformation; and (b) Von-Mises stress contour
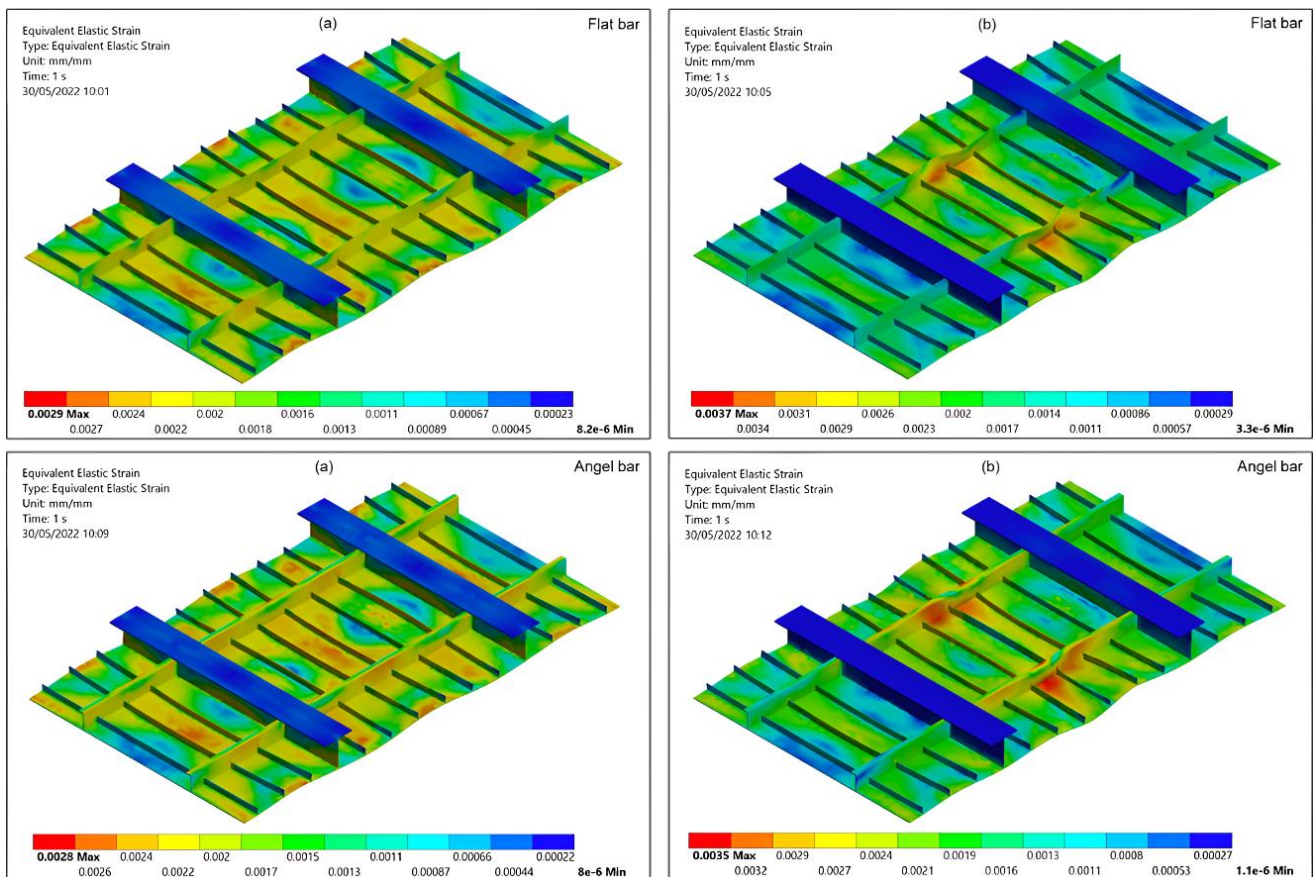
Figure 12. Equivalent strain contour of stiffened panel at the end of simulation: (a) 5 mm displacement; and (b) 10 mm displacement

### 3.2. Displacement and its Effect

Figure 13 displays the results of load versus displacement subjected to 5 mm and 10 mm of displacement for flat, angle, and Tee bar. The increase in displacement does not remarkably affect the load-bearing strength until the maximum compressive strength occurs (Figure 13). It seems that the load versus displacement obtained from 10 mm of displacement is quite different from the 5 mm of displacement. There are some increases in terms of maximum compressive strength obtained from flat bar, angle bar, and Tee bar stiffener types. However, these increments appear to have not been insignificant. Upon observation, it becomes evident that a 10 mm displacement yields the maximum compressive strength for stiffened panels, considering various types of stiffeners, namely flat, angle, and Tee bar. The numerical values associated with this phenomenon showcase the distinctive responses of each stiffener type, emphasizing the importance of displacement in influencing structural behavior. At the 10 mm displacement mark, the maximum compressive strengths were recorded at 6297.5 kN, 6832.8 kN, and 7292 kN for the flat, angle, and Tee bar stiffeners, respectively. In contrast, at a 5 mm displacement, the compressive strength does not reach its peak for any of the aforementioned stiffener types. The corresponding compressive strengths at 5 mm were measured at 6191.3 kN, 6702.2 kN, and 7176 kN for flat, angle, and Tee bars, respectively. This intriguing phenomenon highlights a substantial difference of approximately 106.2 kN, 130.6 kN, and 116 kN, manifesting as larger compressive strengths at the 10 mm displacement compared to the 5 mm displacement for flat, angle, and Tee bar type stiffeners, respectively. This nuanced comparison underscores the sensitivity of the stiffened plates to varying displacements and offers valuable insights into the nuanced mechanical responses dictated by different stiffener configurations under distinct loading conditions.
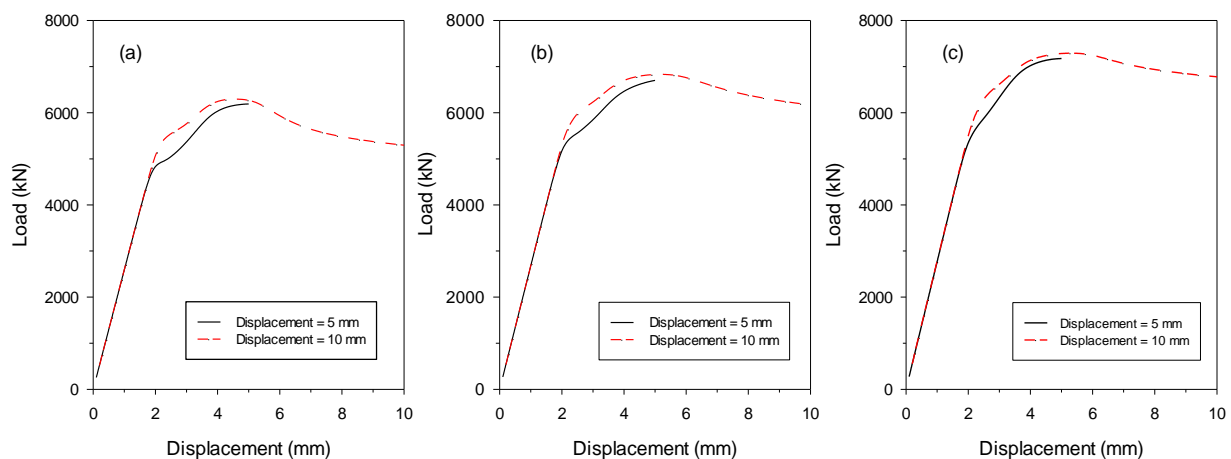
Figure 13. The ultimate strength characteristics of a reinforced panel subjected to biaxial compression involve evaluating three configurations: (a) Flat; (b) Angle; and (c) Tee bar

The comparative analysis of stress average behavior for stiffened panels subjected to 5 mm and 10 mm displacements, considering flat, angle, and Tee bar configurations, is intricately depicted in Figure 14. The stress average behavior manifests itself around 250.81 MPa, 254.08 MPa, and 249.8 MPa for stiffened panels featuring flat, angle, and Tee bars, respectively, when subjected to a 5 mm displacement. In contrast, under a 10 mm displacement, the maximum stress averages approximately 240.66 MPa, 249.71 MPa, and 255.94 MPa, sequentially, for the corresponding stiffened

panel configurations. Intriguingly, these findings suggest a nuanced observation, indicating that the maximum stress average does not exhibit a substantial variance between the results obtained from stiffened panels subjected to 5 mm and 10 mm displacements. This subtle distinction prompts a closer examination of the structural response, implying that the impact of displacement magnitude on stress average may not be as pronounced as anticipated. The convergence of stress averages across the two displacement scenarios raises intriguing questions about the inherent structural characteristics and response patterns of stiffened panels, warranting a more in-depth investigation into the underlying factors influencing their behavior under varying displacement conditions.
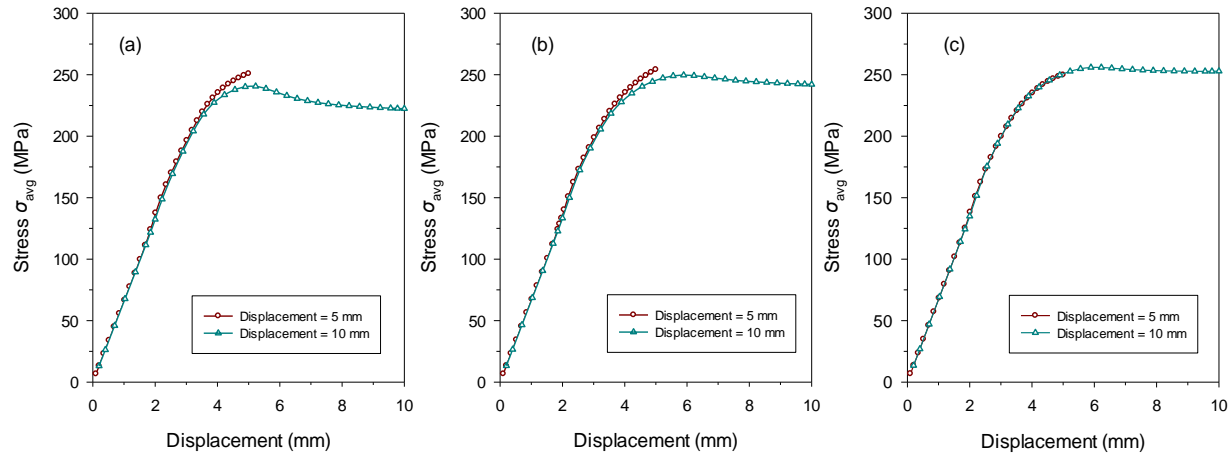
Figure 14. The stress average behavior for the stiffened panel under biaxial compression: (a) Flat; (b) Angle; and (c) Tee bar

3.3. Effect of the Element Size

The finite element method is extremely concerned about proposing the mesh size. The actual structure will be discretized into small elements when using the finite element method. As can be seen in Figures 15 and 16, the mesh size affects the maximum compressive load output on stiffened panels with stiffener type flat, angle, and Tee bar. In this study, it can be seen that the larger the mesh size, the greater the maximum compressive load value. The greater maximum compressive strength value occurs in 5 mm and 10 mm displacement scenarios. For stiffened panels with the Tee bar type itself, the value is 6191.3 kN when a mesh size of 60 mm is obtained from 5 mm displacement. While the results obtained at the 80mm mesh size are at 6544.9 kN. This shows that there is an increase in the maximum compressive strength value of 5.55%. The same phenomenon occurs in the stiffened panel with the other stiffener type which is the angle bar and flat bar. In the analysis encompassing mesh sizes ranging from 60 mm to 80 mm for both types of stiffeners, a discernible increase in maximum compressive strength is observed. Specifically, within this mesh size range, the flat bar stiffener exhibits an approximate increment of 4.56%, reaching a maximum compressive strength value of 6297.5 kN, while the corresponding increase for the angle bar stiffener is approximately 4.13%, resulting in a maximum compressive strength value of 6715.3 kN.
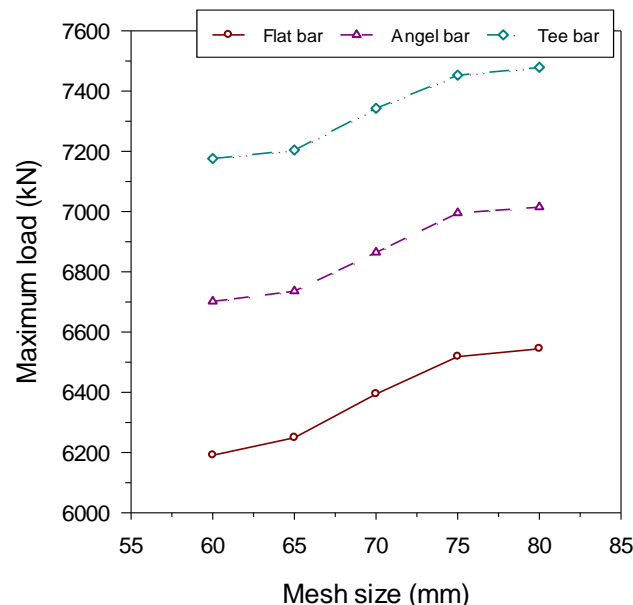
Figure 15. Comparison of the maximum peak strength of stiffened panels obtained from different mesh sizes in 5 mm displacement
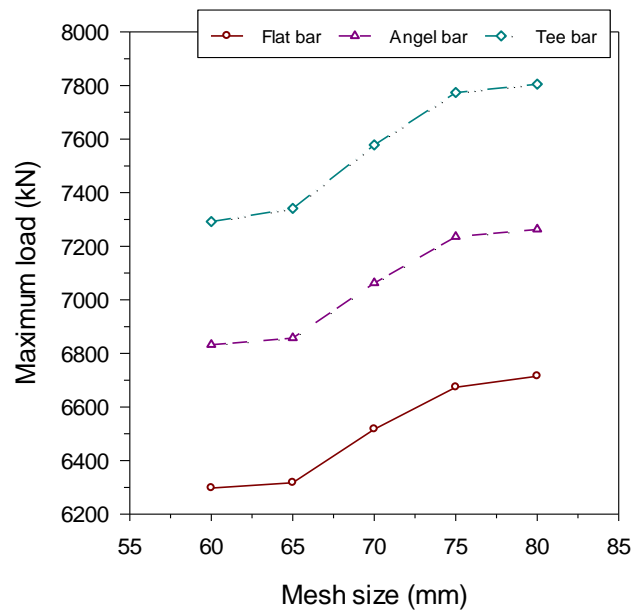
Figure 16. Comparison of the maximum ultimate strength of stiffened panels obtained from different mesh sizes in 10 mm displacement

Furthermore, when subjecting the stiffened panel to a 10 mm displacement, a distinctive divergence in maximum compressive strength values is elucidated for the flat bar stiffener across the specified mesh size range. Notably, the difference in maximum compressive strength values between the 60 mm and 80 mm mesh sizes amounts to 6.42%, signifying a noteworthy variation of 417.8 kN. Specifically, the maximum compressive strength values are recorded at 6297.5 kN and 6715.3 kN for the 60 mm and 80 mm mesh sizes, respectively. This nuanced exploration of the variations in maximum compressive strength under different mesh sizes and displacement conditions provides a comprehensive understanding of the structural performance nuances between the two stiffener types, offering valuable insights for optimizing the design and structural integrity of stiffened plates subjected to buckling loads.

In Figures 17 and 18, a detailed comparison is presented, depicting the average maximum stress levels within stiffened panels that underwent analysis utilizing various mesh sizes and were subjected to displacements of both 5 mm and 10 mm. This investigation reveals a discernible pattern mirroring the trends observed under maximum compressive loads: a direct correlation between the mesh size and the average maximum stress levels. Notably, the findings highlight that as the mesh size increases, there is a corresponding escalation in the average maximum stress. An interesting observation arises when considering a stiffened panel with a Tee bar-type stiffener subjected to a 5 mm displacement, wherein the utilization of a 60 mm mesh size results in an elevated maximum stress level, reaching 249.8 MPa. This nuanced insight underscores the critical role of mesh size in influencing stress distribution and provides valuable information for optimizing numerical simulations for accurate stress predictions in stiffened panels.
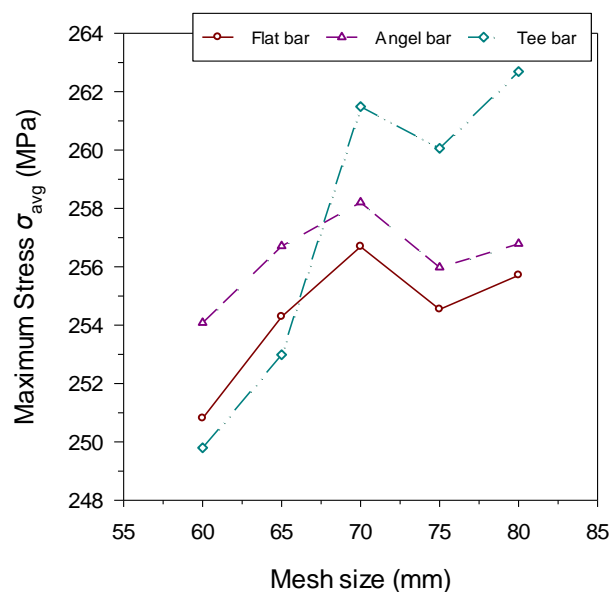

Figure 17. Comparison of the maximum stress average of stiffened panel obtained from different mesh sizes in 5 mm displacement
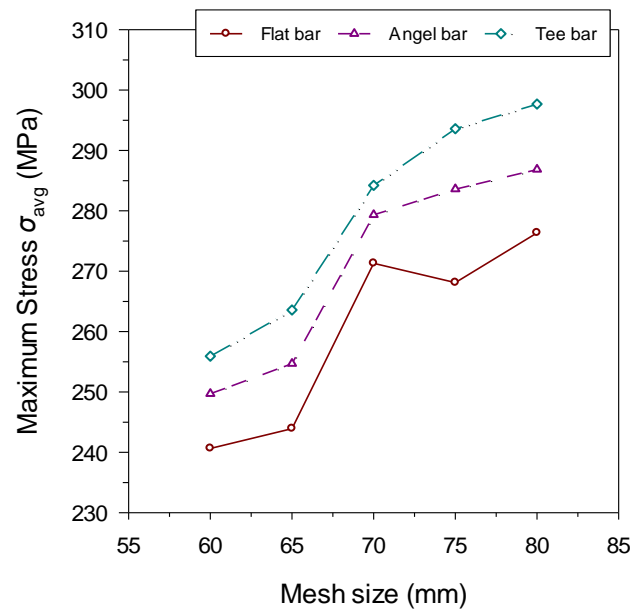
Figure 18. Comparison of the maximum stress average of stiffened paned obtained from different mesh size in 10 mm displacement

Continuing the discussion, it is imperative to emphasize the broader implications derived from the comprehensive analysis of stress patterns within stiffened panels. The exploration of various mesh sizes underlines the intricate relationship between meshing parameters and stress distribution, elucidating crucial nuances that impact the structural response. Figures 17 and 18 not only serve as visual aids but also serve as indispensable tools for researchers and practitioners seeking to enhance the accuracy of finite element simulations in similar structural analyses. Moreover, the specific instance of a Tee bar-type stiffener in a stiffened panel experiencing a 5 mm displacement, yielding a peak stress of 249.8 MPa with a 60 mm mesh size, reinforces the importance of meticulous meshing considerations in capturing localized stress concentrations accurately. This information is invaluable for engineers and designers striving to optimize their simulation models and enhance the predictive capabilities of numerical analyses, ultimately contributing to advancements in the understanding and design of stiffened plate structures under buckling loads.

Meanwhile, the results obtained at the 80 mm mesh size are 262.69 MPa. This shows that there has been an increase in the average maximum stress of 5.03%. The same phenomenon occurs in the other stiffener types, which are the angle bar and flat bar, where the larger the mesh size, the greater the maximum stress average value. Overall, the increase occurred in the range of 1.03% to 1.61% and 1.38%. up to 2.32% of 60-80mm, respectively. Displacement of 10 mm also produces the same phenomenon but has a slightly larger percentage, with a range of maximum increase in average stress reaching 13.81%, 13.85%, and 15.08% for stiffener types flat, angle, and Tee bar, respectively. The selection of the mesh size can indeed produce simulation results with different finite elements. This can be seen in the simulation of stiffened panels with all types of stiffeners subjected to 5 mm displacement at a 75 mm mesh size. In this case, there is a decreasing trend where the maximum stress average value is slightly lower than the 70 mm mesh size. The resulting reductions for the type of stiffener flat, angle, and Tee bar at 70 mm to 75 mm are 256.69 MPa to 254.54 MPa, 258.21 MPa to 255.98 MPa, and 261.49 MPa to 260.06, respectively. It appears that the size of the mesh is crucial in the FE method because the result can be varied along with the size of the mesh.

3.4. Discussion of the Results

A finite element study of the stiffened panel along with the three types of stiffeners subjected to buckling load has been carried out in this study. Stiffened panels are widely used in ship structures. The graph depicting the relationship between load and displacement, as well as the average stress (σ_{avg}), illustrates the ability of the reinforced panel to endure applied loads. The FE results suggest that the stiffener type appears to affect the strength stiffened panel when subjected to buckling load. The findings of this study show that the Tee bar type of stiffener leads to good results for the maximum compressive load on the stiffened panel compared to the flat and angle bar when subjected to the buckling phenomenon. A higher value of maximum compressive load means that the structure of the stiffened panel can withstand the load more greatly.

A typical load versus displacement curve is given in Figures 6 and 7. As seen in these curves, the load for some displacement will reach an initial maximum so the stiffened panel is undergoing maximum capacity. This phenomenon of the relationship between load-bearing strength associated with the maximum compressive strength curve of the stiffened panels under biaxial compression is seen in the studies conducted by Omidali & Khedmati [4] and Paik and Seo [3]. The current study is in accordance with both references which show that maximum compressive load can determine the strength of the stiffened panel when subjected to buckling load. As evidenced by the data presented in

Figures 6 and 7, there is a discernible augmentation in the maximum compressive strength by 15.90% and 8.25% for the Tee bar and angle bar stiffener types, respectively, when subjected to a 5 mm displacement, as compared to the flat bar. The corresponding numerical values for this increase in compressive strength are noteworthy: the flat bar registers at 6191.3 kN, the angle bar at 6702.2 kN, and the Tee bar at an impressive 7176 kN. Furthermore, it is noteworthy that the load versus displacement relationship obtained from a 10 mm displacement exhibits similarity to the trends observed at the 5 mm displacement, with only marginal differences discernible between the two displacement magnitudes.

In the application of the finite element method in simulation, a comprehensive model of a large structure undergoes segmentation into smaller components referred to as finite elements. These elements establish connections among all the key points situated within their boundaries, known as nodes. The criticality of selecting an appropriate mesh size in the finite element method cannot be overstated, as it plays a vital role in the accuracy and reliability of structural simulations; moreover, the partitioning of this mesh necessitates careful consideration to ensure that the chosen size adequately represents the intricacies of the structure [20-23]. Extensive scholarly discourse in the realm of structural analysis emphasizes the profound impact of mesh size on simulation outcomes [24, 25]. Previous research endeavors have demonstrated that variations in mesh size can yield disparate results, thereby underscoring the need for meticulous attention to this parameter.

Studies by Ridwan et al. [26] and Prabowo et al. [27] have elucidated the multifaceted implications of mesh size, revealing its influence not only on the structural response but also on the formation of fractures within a given structure. The consequential effect on energy absorption further accentuates the intricate interplay between mesh size and structural behavior, emphasizing that the nuanced selection of mesh parameters is paramount for a comprehensive understanding of the simulated phenomena. This intricate relationship between mesh size, structural response, and fracture formation underscores the necessity for a judicious approach in choosing mesh parameters, acknowledging that such choices profoundly shape the fidelity and depth of insights derived from finite element simulations in the study of structures subjected to complex loading conditions. This research also demonstrates that different mesh size produces different peak compressive loads and maximum stress averages in the scenario of stiffened panel subjected to buckling load. In this study, the larger the mesh size, the greater the maximum compressive load and maximum stress average. The greater maximum compressive strength value occurs in the 5 mm and 10 mm displacement scenarios. In the examination of stiffened panels featuring flat, angle, and Tee bar types, it was observed that the maximum compressive strength values, obtained under a 60 mm mesh size and a 5 mm displacement, were 6191.3 kN, 6702.2 kN, and 7176 kN, respectively. Subsequent analysis with an 80 mm mesh size yielded results of 6544.9 kN, 7015.3 kN, and 7479 kN for the same stiffener types. Notably, these results indicate a discernible increase in maximum compressive strength by 5.55%, 4.56%, and 4.13% when compared to the outcomes derived from the 60 mm mesh size. This underlines the sensitivity of buckling loads to mesh size and its impact on the structural response. These results regarding the sensitivity of the mesh size to the maximum compressive strength were in accordance with the study conducted by Pratama et al. [28]. The study further emphasizes the critical role of structure stiffness in determining buckling behavior, elucidating that the T bar stiffener type imparts greater stiffness compared to the angle bar and flat bar stiffeners.

Additionally, the assessment of buckling analysis is acknowledged to be contingent upon factors such as column slenderness ratio and plate slenderness ratio, as elucidated in previous studies [29]. Remarkably, this study does not delve into these ratios, presenting a noteworthy avenue for future research endeavors. While the current investigation provides valuable insights into the comparative performance of stiffeners under varying mesh sizes, future studies could incorporate a more comprehensive analysis by including plate and column slenderness ratios. Furthermore, in the pursuit of advancing maritime safety, it is suggested that interested readers refer to a comprehensive source on the subject found in [30-36]. This not only underscores the interconnectedness of diverse research domains but also implies the potential for integrating findings from this study into broader frameworks for maritime safety enhancement.

4. Conclusion

This study delves into a comprehensive analysis and comparison of the buckling load exhibited by steel stiffened panels, exploring various factors such as stiffener types (flat, angle, and Tee bar), displacement conditions, and mesh size, utilizing the finite element method. The investigation yielded insightful conclusions, highlighting the distinct performance of different stiffener types. Notably, the stiffened panel featuring Tee bar stiffeners demonstrated a remarkable increase in maximum compressive load compared to counterparts with flat and angle stiffener types. Additionally, the angle stiffener type exhibited notably superior performance in terms of load-bearing strength when contrasted with the flat bar. The findings revealed a substantial enhancement in maximum compressive load, with at least a 15.90% and 8.25% increase observed in stiffened panels subjected to a 5 mm displacement for Tee and angle bar stiffener types, respectively, in comparison to the flat bar. Intriguingly, the comparison of load versus displacement between 5 mm and 10 mm displacement scenarios indicated minimal variation, suggesting that a 10 mm displacement does not significantly affect the maximum compressive load in the given stiffened panel boundary conditions. It is noteworthy that this study did not quantify and discuss the impact of welding, a critical element in ship structures where stiffened panels are commonly employed. The absence of an examination of the welding effect underscores the need for future research to comprehensively explore and quantify how welding between stiffeners and plates influences the behavior of these stiffened panels.

In the context of the material utilized in this research, the stiffened panels were constructed using S355JR-EN10210 steel, a high-strength structural steel renowned for its significant mechanical features. S355JR-EN10210 steel is significant in providing confidence about the structural performance and integrity of the stiffened panels under the imposed buckling loads. This steel grade is characterized by its robustness, making it well-suited for applications demanding resilience and strength, such as ship structures. However, while the current study has provided valuable insights into the performance of stiffened panels based on geometric and load considerations, the specific influence of the material's properties, including its response to welding, remains unexplored. Future research endeavors should thus focus on a detailed examination of the use of S355JR-EN10210 steel, considering its welding characteristics and its impact on the overall behavior of stiffened panels. Such an investigation would contribute to a more thorough comprehension of the structural dynamics and performance of stiffened panels, especially in practical applications where welding plays a crucial role in the assembly and integrity of these structural elements. In conclusion, while this study has shed light on critical aspects of stiffened panel behavior, further exploration, particularly regarding the material and welding effects, is essential for advancing the knowledge and application of stiffened panels in engineering and structural design.

5. Declarations

5.1. Author Contributions

Conceptualization, M.S., R.R., A.R.P., and I.Y.; methodology, R.R., A.R.P., and R.A.; software, A.R.P., R.A., and J.M.S.; validation, M.S., R.R., and J.M.S.; formal analysis, M.S., R.R., A.R.P., and I.Y.; investigation, M.S., R.R., A.R.P., and R.A.; resources, A.R.P., T.G.G., and D.D.D.P.T.; data curation, R.R., A.R.P., and R.A.; writing—original draft preparation, M.S., R.R., A.R.P., and I.Y.; writing—review and editing, R.R., A.R.P., and T.G.G.; visualization, T.G.G., N.M., and D.D.D.P.T.; supervision, A.R.P., I.Y., and R.A.; project administration, A.R.P., J.M.S., T.G.G., and N.M.; funding acquisition, A.R.P., N.M., D.D.D.P.T., and J.M.S. All authors have read and agreed to the published version of the manuscript.

5.2. Data Availability Statement

The data presented in this study are available in the article.

5.3. Funding

5.4. Conflicts of Interest

The authors declare no conflict of interest.

6. References

[1] UNCTAD. (2021). Review of Maritime Transport 2021. United Nations Conference on Trade and Development, United Nations Publication, Geneva, Switzerland.

[2] Allianz. (2021). Safety and shipping review 2021. Allianz Global Corporate & Specialty, Munich, Germany.

[3] Paik, J. K., & Seo, J. K. (2009). Nonlinear finite element method models for ultimate strength analysis of steel stiffened-plate structures under combined biaxial compression and lateral pressure actions-Part II: Stiffened panels. Thin-Walled Structures, 47(8–9), 998–1007. doi:10.1016/j.tws.2008.08.006.

[4] Omidali, M., & Khedmati, M. R. (2018). Reliability-based design of stiffened plates in ship structures subject to wheel patch loading. Thin-Walled Structures, 127, 416–424. doi:10.1016/j.tws.2018.02.022.

[5] Doan, V. T., Liu, B., Garbatov, Y., Wu, W., & Guedes Soares, C. (2020). Strength assessment of aluminium and steel stiffened panels with openings on longitudinal girders. Ocean Engineering, 200(107047). doi:10.1016/j.oceaneng.2020.107047.

[6] Pedram, M., & Khedmati, M. R. (2014). The effect of welding on the strength of aluminium stiffened plates subject to combined uniaxial compression and lateral pressure. International Journal of Naval Architecture and Ocean Engineering, 6(1), 39–59. doi:10.2478/IJNAOE-2013-0162.

[7] Guedes Soares, C., & Gordo, J. M. (1997). Design Methods for Stiffened Plates under Predominantly Uniaxial Compression. Marine Structures, 10(6), 465–497. doi:10.1016/s0951-8339(97)00002-6.

[8] Feng, L., Yu, J., Zheng, J., He, W., & Liu, C. (2024). Experimental and numerical study of residual ultimate strength of hull plate subjected to coupled damage of pitting corrosion and crack. Ocean Engineering, 294. doi:10.1016/j.oceaneng.2024.116710.

[9] Cui, J., & Wang, D. (2020). An experimental and numerical investigation on ultimate strength of stiffened plates with opening and perforation corrosion. Ocean Engineering, 205. doi:10.1016/j.oceaneng.2020.107282.

[10] Lee, J., & Kang, Y. J. (2024). Elastic local buckling coefficients of I-shaped beams considering flange–web interaction. Thin-Walled Structures, 195. doi:10.1016/j.tws.2023.111325.

[11] Boissonnade, N., Nseir, J., & Somja, H. (2024). Experimental and numerical investigations towards the lateral torsional buckling of cellular steel beams. Thin-Walled Structures, 195. doi:10.1016/j.tws.2023.111388.

[12] Ghadami, A., Jawdhari, A., & PourMoosavi, G. (2024). Buckling and post-buckling behavior of top flange coped I-beams with slender web panels. Thin-Walled Structures, 198(111640). doi:10.1016/j.tws.2024.111640.

[13] Quinn, D., Murphy, A., McEwan, W., & Lemaitre, F. (2009). Stiffened panel stability behaviour and performance gains with plate prismatic sub-stiffening. Thin-Walled Structures, 47(12), 1457–1468. doi:10.1016/j.tws.2009.07.004.

[14] Esmaeili-Goldarag, F., Babaei, A., & Jafarzadeh, H. (2018). An experimental and numerical investigation of clamping force variation in simple bolted and hybrid (bolted-bonded) double lap joints due to applied longitudinal loads. Engineering Failure Analysis, 91, 327–340. doi:10.1016/j.engfailanal.2018.04.047.

[15] Goldarag, F. E., Barzegar, S., & Babaei, A. (2015). An experimental method for measuring the clamping force in double lap simple bolted and hybrid (bolted-bonded) joints. Transactions of Famena, 39(3), 87–94.

[16] ANSYS. (2020). ANSYS LS-DYNA User's Guide. ANSYS Inc., Pennsylvania, United States.

[17] Ridwan, Putranto, T., Laksono, F. B., & Prabowo, A. R. (2020). Fracture and damage to the material accounting for transportation crash and accident. Procedia Structural Integrity, 27, 38–45. doi:10.1016/j.prostr.2020.07.006.

[18] Prabowo, A. R., Tuswan, T., Prabowoputra, D. M., & Ridwan, R. (2021). Deformation of designed steel plates: An optimisation of the side hull structure using the finite element approach. Open Engineering, 11(1), 1034–1047. doi:10.1515/eng-2021-0104.

[19] Dzulfiqar, M. F., Prabowo, A. R., Ridwan, R., & Nubli, H. (2021). Assessment on the designed structural frame of the automatic thickness checking machine - Numerical validation in FE method. Procedia Structural Integrity, 33, 59–66. doi:10.1016/j.prostr.2021.10.009.

[20] Prabowo, A. R., Ridwan, R., Tuswan, T., Sohn, J. M., Surojo, E., & Imaduddin, F. (2022). Effect of the selected parameters in idealizing material failures under tensile loads: Benchmarks for damage analysis on thin-walled structures. Curved and Layered Structures, 9(1), 258–285. doi:10.1515/cls-2022-0021.

[21] Ridwan, R., Nuriana, W., & Prabowo, A. R. (2022). Energy absorption behaviors of designed metallic square tubes under axial loading: Experiment-based benchmarking and finite element calculation. Journal of the Mechanical Behavior of Materials, 31(1), 443–461. doi:10.1515/jmbm-2022-0052.

[22] Alwan, F. H. A., Prabowo, A. R., Muttaqie, T., Muhayat, N., Ridwan, R., & Laksono, F. B. (2022). Assessment of ballistic impact damage on aluminum and magnesium alloys against high velocity bullets by dynamic FE simulations. Journal of the Mechanical Behavior of Materials, 31(1), 595–616. doi:10.1515/jmbm-2022-0064.

[23] Prabowo, A. R., Ridwan, R., & Muttaqie, T. (2022). On The Resistance to Buckling Loads of Idealized Hull Structures: FE Analysis on Designed-Stiffened Plates. Designs, 6(3), 46. doi:10.3390/designs6030046.

[24] Saleh, S. M., Majeed, F. H., Al-Salih, O., & Hussain, H. K. (2023). Torsional Behavior of Steel-Concrete-Steel Sandwich Beams with Welded Stirrups as Shear Connectors. Civil Engineering Journal, 9(1), 208-219. doi:10.28991/CEJ-2023-09-01-016.

[25] Prabowo, A. R., Do, Q. T., Cao, B., & Bae, D. M. (2020). Land and marine-based structures subjected to explosion loading: A review on critical transportation and infrastructure. Procedia Structural Integrity, 27, 77–84. doi:10.1016/j.prostr.2020.07.011.

[26] Ridwan, R., Prabowo, A. R., Muhayat, N., Putranto, T., & Sohn, J. M. (2020). Tensile analysis and assessment of carbon and alloy steels using Fe approach as an idealization of material fractures under collision and grounding. Curved and Layered Structures, 7(1), 188-198. doi:10.1515/cls-2020-0016.

[27] Prabowo, A. R., & Bae, D. M. (2019). Environmental risk of maritime territory subjected to accidental phenomena: Correlation of oil spill and ship grounding in the Exxon Valdez's case. Results in Engineering, 4(100035). doi:10.1016/j.rineng.2019.100035.

[28] Pratama, A. A., Prabowo, A. R., Muttaqie, T., Muhayat, N., Ridwan, R., Cao, B., & Laksono, F. B. (2023). Hollow tube structures subjected to compressive loading: implementation of the pitting corrosion effect in nonlinear FE analysis. Journal of the Brazilian Society of Mechanical Sciences and Engineering, 45, 143. doi:10.1007/s40430-023-04067-3.

[29] Branquinho, M. Á., & Malite, M. (2021). Effective slenderness ratio approach for thin-walled angle columns connected by the leg. Journal of Constructional Steel Research, 176, 106434. doi:10.1016/j.jcsr.2020.106434.

[30] Demirci, S. M. E., & Elçiçek, H. (2023). Scientific awareness of marine accidents in Europe: A bibliometric and correspondence analysis. Accident Analysis and Prevention, 190, 107166. doi:10.1016/j.aap.2023.107166.

[31] Chen, J., Di, Z., Shi, J., Shu, Y., Wan, Z., Song, L., & Zhang, W. (2020). Marine oil spill pollution causes and governance: A case study of Sanchi tanker collision and explosion. Journal of Cleaner Production, 273, 122978. doi:10.1016/j.jclepro.2020.122978.

[32] Guimarães, L. S. F., de Carvalho-Junior, L., Façanha, G. L., Resende, N. da S., Neves, L. M., & Cardoso, S. J. (2023). Meta-analysis of the thermal pollution caused by coastal nuclear power plants and its effects on marine biodiversity. Marine Pollution Bulletin, 195, 115452. doi:10.1016/j.marpolbul.2023.115452.

[33] Prabowo, A. R., Cahyono, S. I., & Sohn, J. M. (2019). Crashworthiness assessment of thin-walled double bottom tanker: A variety of ship grounding incidents. Theoretical and Applied Mechanics Letters, 9(5), 320–327. doi:10.1016/j.taml.2019.05.002.

[34] Yildiz, S., Uğurlu, Ö., Wang, J., & Loughney, S. (2021). Application of the HFACS-PV approach for identification of human and organizational factors (HOFs) influencing marine accidents. Reliability Engineering and System Safety, 208, 107395. doi:10.1016/j.ress.2020.107395.

[35] Bolat, P., & Yongxing, J. (2013). Risk assessment of potential catastrophic accidents for transportation of special nuclear materials through Turkish Straits. Energy Policy, 56, 126–135. doi:10.1016/j.enpol.2012.12.010.

[36] Cao, B., Bae, D.-M., Sohn, J.-M., Prabowo, A. R., Chen, T. H., & Li, H. (2016). Numerical Analysis for Damage Characteristics Caused by Ice Collision on Side Structure. Volume 8: Polar and Arctic Sciences and Technology; Petroleum Technology, OMAE2016-54727, 1-7. doi:10.1115/omae2016-54727.